Title

Electron Paramagnetic Resonance Characteristics and Crystal Structure of a Tutton Salt Analogue: Copper-Doped Cadmium Creatininium Sulfate

Journal

The Journal of Physical Chemistry A, 124(11)

ISSN

1089-5639

Authors

Colaneri, Michael J

Teat, Simon J

Vitali, Jacqueline

Publication Date

2020-03-19

DOI

10.1021/acs.jpca.0c00004

Electron Paramagnetic Resonance Characteristics and Crystal Structure of a Tutton Salt Analog: Copper Doped Cadmium Creatininium Sulfate

Michael J. Colaneri[†*], Simon J. Teat[§] and Jacqueline Vitali[‡*]

Department of Chemistry and Physics, State University of New York at Old Westbury, Old Westbury, New York 11568, Lawrence Berkeley National Lab, 1 Cyclotron Road MS 15RO317, Berkeley, CA 94720, Department of Physics and Department of Biological, Geological and Environmental Sciences, Cleveland State University, Cleveland, Ohio 44115

*Authors to whom correspondence should be addressed. E-mail: colanerim@oldwestbury.edu Mailing Address: Department of Chemistry and Physics, SUNY at Old Westbury, Old Westbury, NY 11568, USA, Tel: (516) 876-2756. E-mail: j.vitali@csuohio.edu Mailing Address: Department of Physics and Department of Biological, Geological and Environmental Sciences, Cleveland State University, Cleveland, OH 44115, USA, Tel: (216) 687-2431.

†SUNY at Old Westbury.

§Lawrence Berkeley National Lab.

‡Cleveland State University.

Abstract

Electron Paramagnetic Resonance and crystallographic studies on copper-doped cadmium creatininium sulfate (CdCrnS) were undertaken to study the characteristics of a copper-hexahydrate complex in an organic analog of Tutton's salt. X-ray diffraction experiments determined the crystal structure of CdCrnS at both 100 K and 298 K. CdCrnS, like Tutton salt, crystallizes in the monoclinic space group $P2_1/n$. The unit cell contains two cadmium hexahydrate complexes, four creatininium ions, four sulfates and four additional solvation waters. Both crystallography and EPR find the doped copper replaces the cadmium in the structure. Single crystal EPR measurements at room temperature determined the **g** and copper hyperfine ($\mathbf{A^{Cu}}$) tensors (principal values: **g**; 2.437, 2.134, 2.080, $\mathbf{A^{Cu}}$; -327, -84.8, 7.33 MHz). EPR spectra of the powder at room temperature gave **g**; 2.448, 2.125, 2.085 and $\mathbf{A^{Cu}}$; -315, -75.0, 35.0 MHz, and at 110 K gave **g**; 2.462, 2.116, 2.077 and $\mathbf{A^{Cu}}$; -340, -30.0, 35.0 MHz. The room temperature tensors are close to the "rigid lattice limit" values found in copper doped Tutton salts but having a higher g_{min} and weaker A^{Cu}_x coupling than average. A small but measureable temperature dependency of the tensors indicated the presence of a dynamic Jahn-Teller (JT) effect. In addition, the EPR linewidth changed dramatically with temperature which is like that found in all copper doped Tutton crystals. Utilizing the model of Silver-Getz for the g-value variation gave an estimate for the energy difference (δ_{12} = 640 cm^{-1}) between the ground and next highest JT configuration. An empirical correlation appears to exist between δ_{12} and g_{min} and A^{Cu}_x for the copper hexahydrates studied in similar crystals. This suggests a relationship between the amount of unpaired spin in the copper d orbital x-lobe and the gap between wells of the adiabatic potential surface.

Introduction

Our continued interest in the study of metal dynamics in biological models led to a combined crystallographic and Electron Paramagnetic Resonance (EPR) investigation of copper doped cadmium creatininium sulfate (CdCrnS) crystals. The crystal is a metal organic hybrid that has structural features similar to that found in the inorganic double metal sulfate hexahydrates $M^{+}_2M^{2+}(SO_4)_2{\cdot}6H_2O$ or Tutton's salt. Crystallography shows that the doped copper substitutes for cadmium in the hexahydrate complex of the asymmetric unit. This is consistent with alignment of the EPR magnetic tensors with the three metal-water bonds directions. EPR results on CdCrnS show characteristics both typical and atypical to those found for $Cu^{2+}(H_2O)_6$ in doped Tutton salts. One shared feature is an EPR spectral averaging over a range of temperatures, which is the consequence of the dynamic Jahn-Teller (JT) effect[1-5]. In this work, EPR was used to study the dynamic behavior of copper hexahydrate in CdCrnS and to compare findings with results found in similarly doped crystals.

The dynamic JT effect was initially recognized as due to rapid exchange between elongated tetragonal distortions in high symmetry (trigonal) Cu^{2+} sites[5,6] and was later extended to include the lower symmetry D_{2h} copper hexahydrate complexes found in Tutton salts[1-5]. In both situations EPR spectral averaging occurs as a function of temperature. In the former, thermally activated exchange of the three energetically equivalent, static JT distorted sites average the spectra[5,6]. In the latter, the process is multifaceted[1-5]. JT couplings and lattice strains generate three nonequivalent configurations associated with distortions of the three different copper-water bonds. The lowest energy configuration produces rhombic **g** and copper hyperfine ($\mathbf{A}^{\mathbf{Cu}}$) tensors, where the g_{min}, g_{mid} and g_{max} directions are associated with the shortest (x), middle (y) and longest (z) copper-water bonds[1,3,4,7]. These values are the rigid lattice limit tensors.

Orthorhombic strains perturb the energy of the three copper configurations and act to alter the lengths of the metal-water bonds. The potential energy surface contains three valleys of different depths corresponding to the three possible metal-water distortions or JT configurations, of the complex[1,3-5]. The energy difference between the first and second valley is denoted as δ_{12} and the first and third by δ_{13}. Silver and Getz[1] applied a simple dynamic model (SG) to explain how the EPR **g** and $\mathbf{A^{Cu}}$ tensors of copper-doped zinc potassium sulfate hexahydrate (ZKH) vary with temperature. Here, only the deepest well is populated at low temperature. As the temperature rises, with fast transitions between them, the higher wells become populated. In the SG view, these higher states represent simple orientation isomers of the magnetic tensor axes, with the EPR parameters in the three wells being identical. The temperature variation of the EPR tensor parameters then depend on the weighted average of the three orientations of the tensors according to the Boltzmann populations of the three wells.

It is usually observed in the doped Tutton salts that as the temperature rises, g_{min} remains relatively constant while the g_{max} and g_{mid} values approach each other[1,2]. This means that only the two lowest wells become populated at these temperatures, as the third is too high in energy to significantly affect the spectra[1,2]. The tensor y and z components are then the Boltzmann weighted averages of their rigid lattice values, so by measuring their variation with temperature, the energy separation δ_{12} between the two wells can be determined. Using this approach, Silver and Getz were able to successfully explain the variation of the **g** and $\mathbf{A^{Cu}}$ tensors in ZKH, finding an energy difference δ_{12}=75cm^{-1} between the lowest two valleys[1]. This work was soon followed by similar SG analysis of this fluxation behavior of $Cu^{2+}(H_2O)_6$ in other Tutton salts[2,4,8-16] and analogs[17,18], and found δ_{12} values ranging from ~75cm^{-1}-300cm^{-1} for the magnetically dilute crystals and ~300cm^{-1}-500cm^{-1} for the pure copper Tutton crystals.

Several of these EPR studies revealed limitations of the SG model, the most apparent being that δ_{12} is not constant over the entire temperature range[2,4,9,12-15]. In other systems, the tensor variations that were not fully predicted,[4,11,18] which was initially suggested as due to a non-Boltzmann thermal equilibrium at low temperatures, but later also from temperature dependent changes in the lattice strains. In a few other cases, g_{min} was observed to vary with temperature[4,9] and therefore a three-state SG model was applied[1,9,10].

Highlighting the need to rectify some of the limitations of the SG approach, Riley et al.[3] proposed a more advanced dynamic model where higher vibration effects along with JT coupling and lattice strain were included in the Hamiltonian. In their model, the magnetic tensors average over a Boltzmann distribution of the vibration levels of the wells. The inclusion of lattice strain parameters generally led to better agreements to the g-tensor variations, but also found good comparisons with the δ_{12} values that were estimated from the SG model[3,15,19]. However, three systems; the Magnesium Ammonium Tutton salt (abbreviated $MgNH_4S$)[4], the Zinc Ammonium Tutton salt (abbreviated $ZnNH_4S$)[11] and the Tutton analog, $Cs_2Zn(H_2O)_6(ZrF_6)_2$[18] exhibited behaviors inconsistent with either the SG or vibronic models. These failures were attributed to host dynamics of the NH_4 groups and/or fluxations in the hydrogen bonding interactions, leading to temperature dependent deformations of the potential energy surfaces[11,18,21]. Keeping in mind the restricted temperature validity of the SG model in most of these systems, the δ_{12} values used in discussions below were those reported in ranges where they remained relatively constant, i.e., usually when T>120 K.

This study of CdCrnS gives the first opportunity to evaluate copper dynamic behavior in a metal organic hybrid analog of Tutton's salt. One focus is to evaluate how results from this system fit into the larger body of conclusions derived from studies on Tutton salts. In general,

EPR studies of small molecule crystal systems are particularly advantageous because they provide insights into how dynamics are related to the nature of the unpaired electron wavefunction. They can also add valuable information on the geometric structure of different states which interconvert and may ultimately help interpret the role of copper motions in the function of important biological molecules[22-26]. In addition, the current study complements our earlier EPR investigations on copper-histidine complexes whose temperature dependent spectra were could be explained as a motional averaging between neighboring metal binding sites [27-29].

Experimental

Single crystals of copper-doped cadmium creatininium sulfate were grown by slow evaporation of aqueous solutions containing creatinine and cadmium sulfate, with a small ~1-3% amount of copper sulfate. The prismatic crystals were pale blue. All compounds were of highest purity obtained from Fisher Scientific and Sigma-Aldrich.

Crystallography

X-ray diffraction data were collected on a single crystal using a Bruker D8 diffractometer equipped with a PHOTONII detector and operating with a silicon 111 monochromator and synchrotron radiation of wavelength 0.7288 Å at 298(2) K and 100(2) K at beamline 12.2.1 of the Advanced Light Source at Lawrence Berkeley National Laboratory. The scans were shutterless. The same crystal was used for both data collections. The Bruker Apex 3 program was used for the data collection[30]. Intensity data integrations, cell refinement, and data reduction were performed using the Bruker SAINT software package[30]. Absorption correction was made with SADABS[30, 31]. Crystal data are given in Table 1.

The 298 K structure was determined with direct methods using SHELXT 2014[32] and refined using SHELXL 2018[32]. All non-hydrogen atoms were refined anisotropically. During

refinement, the positions and displacement parameters of Cd and Cu were constrained to be the same at the inversion center and their occupancies refined with their sum constrained to be 0.5. Hydrogen atoms were obtained from electron density difference maps and allowed to refine freely except for the methyl group where geometry constraints were used. The same procedure was adopted for the 100 K structure. Data collection and refinement details for both structures are given in Table 1. Further details, including atomic parameters, complete distances and angles and hydrogen bonds are found in the Supporting Information. Superpositions were carried out with Olex2[33] (https://www.olexsys.org). Figures were prepared with ORTEP-3[34], Chimera[35] and OLEX2[33].

EPR Spectroscopy

The CW-EPR measurements were carried out using a Varian X-band E-109 spectrometer interfaced to a PC and gaussmeter as described in the past[27-29]. DPPH (g=2.0036) was used as a g-value reference. An ESR900 Oxford Cryostat system employing liquid nitrogen was utilized for the variable temperature experiments. Crystals were mounted with duco cement on long Pasteur pipettes, inserted in standard 3 x 4 mm EPR quartz tubes and affixed to a Bruker goniometer. The **a**, **b** and **c'** axes (**c'** = **a** x **b**) were used as the reference system for the EPR rotation measurements. Some crystals were manually crushed into powders and placed directly in the tubes. The **g** and copper hyperfine ($\mathbf{A}^{\mathbf{Cu}}$) tensors were determined by a least-square fit of the spectral data to the spin Hamiltonian (Equation 1) using methods outlined before (29).

Equation 1
$$\mathcal{H} = \beta S \bullet g \bullet H - I \bullet A^{Cu} \bullet S - g_n \beta_n H \bullet I + I \bullet Q \bullet I,$$

with S=1/2, I=3/2, and remaining terms defined in the usual way[36]. In Equation 1, the inclusion of a copper nuclear quadrupole tensor (**Q**) of (20, -10, -10 MHz)[37], produced a better fit of the data. EasySpin[38] was employed to simulate the powder EPR patterns and gnuplot was used to fit

the spectral linewidth dependence on temperature.

Results

Description of the Structures

As seen in Table 1, upon cooling the unit cell slightly shrinks along **b** by 0.1696(15) Å and along **a** and **c** by 0.0302(4) Å and 0.0398(4) Å, respectively. Matching of all parts of the asymmetric unit with OLEX2 gives rms of 0.123 Å for creatininium, 0.023Å for the metal hexahydrate and 0.007 Å for the sulfate. As expected, the temperature factors are lower at 100 K.

The asymmetric unit consists of a creatininium cation, a sulfate, 3 waters coordinated to a mixed Cd/Cu site at the inversion center and one solvation water (Figure 1). The Cd/Cu site is coordinated by six waters, three from the asymmetric unit and three from its centrosymmetrically related mate. The asymmetric unit shown in Figure 1 is expanded by symmetry to include the coordination of the Cd/Cu site at the inversion center. The Cd/Cu site adopts a slightly distorted octahedral coordination geometry. Bond lengths and angles are presented in Tables S3 and S9 for the 298 K and 100 K structures, respectively. This coordination of the metal site by six waters is similar to that seen in metal hexahydrate complexes of Tutton's salts[39] and other structural analogs of them with organic cations[40-44]. The Cd/Cu - OW bonds are in the range 2.2295(8) to 2.3178(7) Å at 298 K and 2.2322(7) to 2.3124(7) at 100 K. The cis OW-Cd/Cu-OW angles range from 91.95(4) to 93.36(3)° at 293 K and 91.95 to 93.91(3) at 100K. The trans OW-Cd/Cu-OW angles are 180° by the crystallographic inversion center. The average Cd-OW

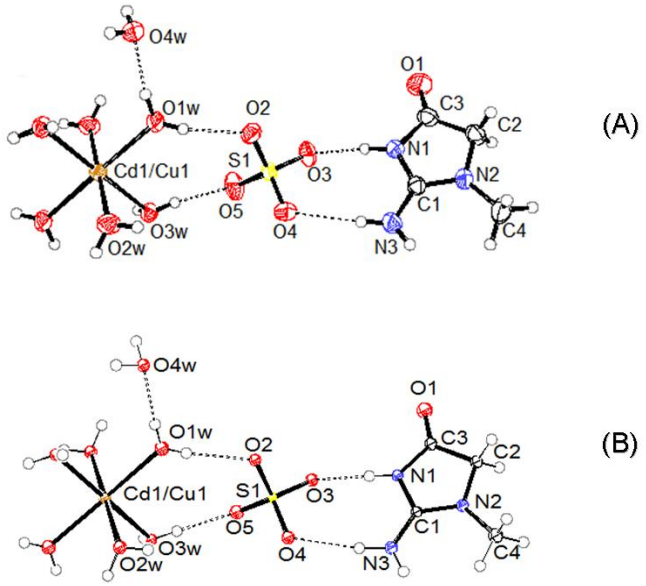

Figure 1

distance of 2.269 is like cadmium ammonium sulfate hexahydrate[45]. The creatininium ring is planar, as expected, with a rmsd of 0.007 Å (0.008 Å at 100 K). Bond distances and angles are comparable to other creatininium cations[46-49]. Hydrogen bonds are given in Tables S6 and S12. The structure is held together by a network of hydrogen bonds and stacking interactions. The Cd/Cu $[(H_2O)_6]^{2+}$ cations form layers perpendicular to the **b** axis that consist of columns of the cations along **a**, **c** and along **a** + **c**. In between these cation columns are columns of solvation waters. The Cd/Cu $[(H_2O)_6]^{2+}$ cation layer is flanked by a layer of sulfate anions in each side. The creatinine cations make a double layer adjacent to the sulfate layers on the other side of the inorganic cation layer. This arrangement looking down **a** axis parallel to **b** is illustrated in Figure 2. The Cd cations are connected via hydrogen bonds with the solvation water and with the adjacent sulfates. The creatininiums also connect the adjacent sufates in their layer and in the layer across of them via hydrogen bonds. The only hydrogen

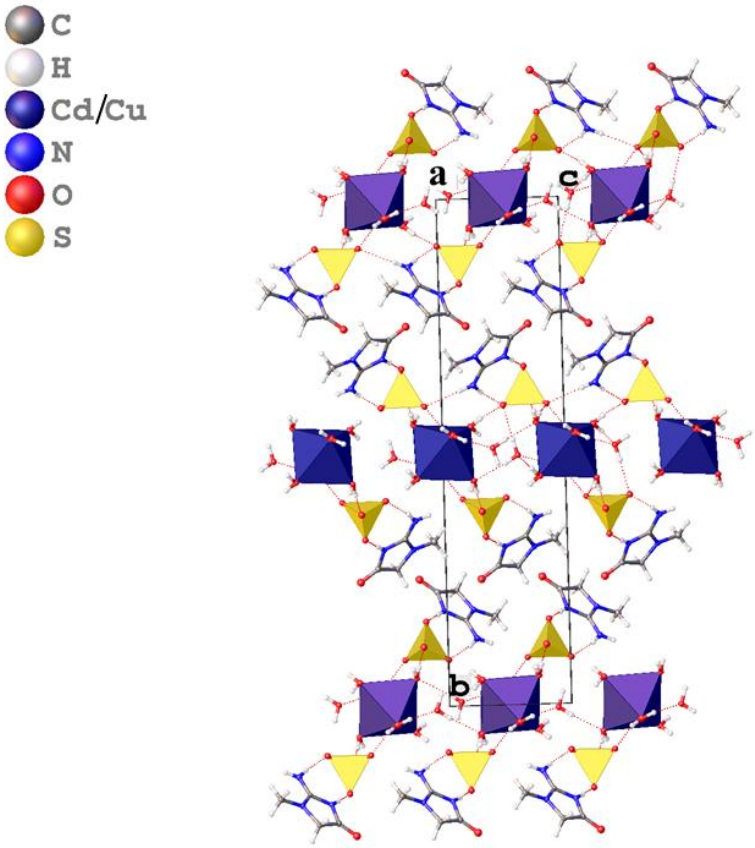

Figure 2

bonding interaction between creatininiums in the same layer is a C4-H…O1 hydrogen bond (Tables S6 and S12). Creatininiums in the same layer do not form pi-pi interactions. Instead the sulfates of the adjacent sulfate layer along **a** form stacking interactions with the creatininiums (Figure 3). The shortest distances of the sulfate oxygens to the creatininium ring in these interactions are O5 ---C1 3.305 A (3.262 Å at 100 K) O5---C3 3.385 Å (3.360 Å at 100 K) and O3---C2 3.285 Å (3.244 Å at 100 K). Similar vertical interactions between creatininium cations and anions have been observed with the nitrate oxygens in creatininium nitrate[50] and with the sulfate oxygens in bis(creatininum)sulfate[46]. Anion-π interactions are common[51] and exist also in proteins and nucleic acids[53] providing stabilization. The

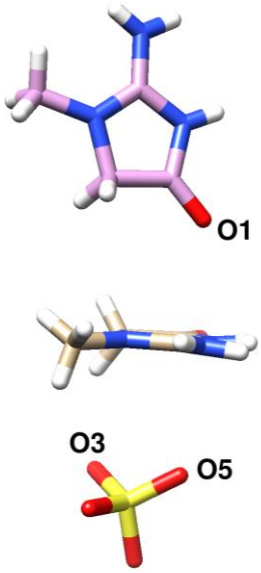

Figure 3

two creatinine layers are at an angle 81.97° (80.95° at 100K) to each other and interact with a vertical stacking interaction in which O1 of the creatinines of one layer overlap the rings of the other with closest distances of O1---C1 3.006 Å (2.956 Å at 100 K), O1---C3 3.312 Å (3.274 Å at 100 K) and O1 … N2 3.343 Å (3.306 Å at 100 K). Similar edge-on stacking interactions between two creatininiums involving O1 have been observed in creatininium nitrate[50] and are analogous to anion-π interactions.

EPR Measurements

Single crystal CW-EPR spectra show signals with the characteristic quartet hyperfine pattern arising from a Cu^{2+} (I=3/2) coupling. Figure 4 shows the EPR when the magnetic field **H** is directed along the **a**, **b** and **c'** axes. The copper m_I lines are broad and lack any resolved hyperfine splitting. Only one resonance pattern is visible when the external field (**H)** lies in the crystallographic **ac'** plane, and this pattern site-splits into two when **H** is directed in the **ab** and

bc' planes. This is consistent with having a single copper centered complex in the

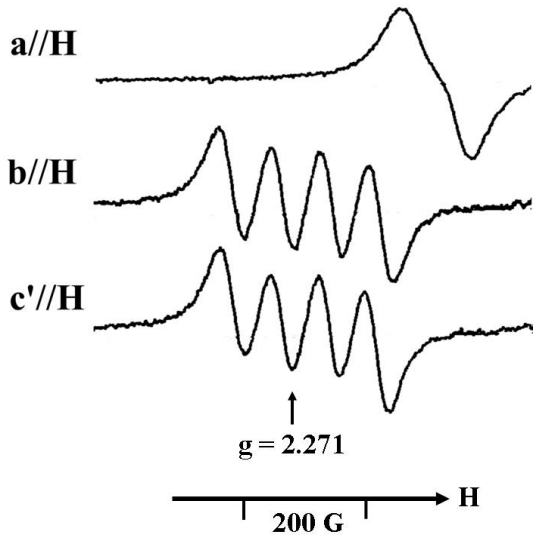

Figure 4

asymmetric unit. The midpoint of the pattern at both the **b**//**H** and at **c'**//**H** orientations are g=2.271 with a resolved copper hyperfine splitting. The splitting almost entirely collapses at **a**//**H** as the g-value decreases. The linewidths of the individual single crystal resonance peaks remain nearly constant at ~35 G.

The EPR resonant fields are plotted in Figure 5 as the crystal was rotated with respect to the external magnetic field direction in the three reference planes. The refined **g** and copper hyperfine ($\mathbf{A}^{Cu}$) tensors fit to the data are listed in Table 2. The least-square calculation terminated when the goodness-of-fit fell below 4.5 G (~15 MHz). The copper hyperfine values were assumed to have similar errors. The solid blue curves in the Figure display how the theoretical fields vary with crystal orientation using best-fit parameters in Equation 1.

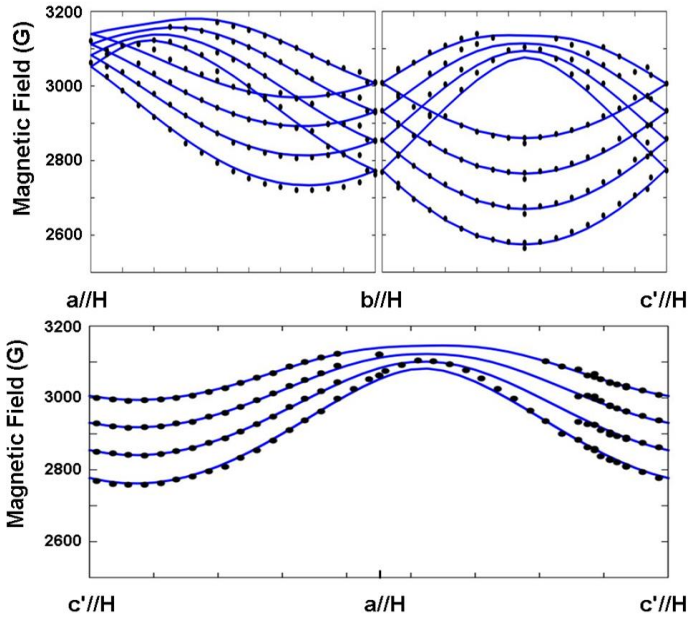

Figure 5

The single crystal **g** and $\mathbf{A}^{Cu}$ tensors are rhombic (principal values: **g**; 2.437, 2.134, 2.080, $\mathbf{A}^{Cu}$; -327, -84.8, 7.33 MHz) and share the same principal frame having a maximum angular difference of ~6°. A good correlation is found between the tensor axes and directions of the metal-water bonds in the crystal structure. The copper hexahydrate complex is depicted in Figure 6. The deviations (δ°: 1.6°, 6.0°, 7.9°) between the **g** tensor and the metal-OW directions are small and within normal error limits for X-band single crystal measurements[27,29]. The tensor axes are consistent with those found in previous studies of $Cu^{2+}(H_2O)_6$ in Tutton salts[1,3,7-9]. The metal-water bond lengths in Figure 6 are those of the host CdCrnS structure. These change for the copper due to the JT distortion and other strains exerted by the host lattice,

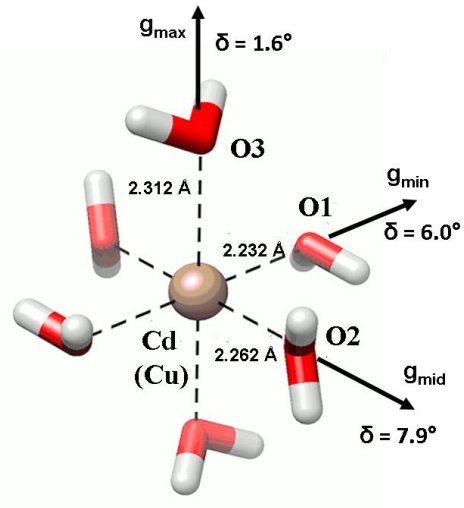

Figure 6

so that the longest, middle and shortest Cu-OW bond lengths correlate with the g_{max} (g_z), g_{mid} (g_y) and g_{min} (g_x) tensor values, respectively. The room temperature tensor values (**g**; 2.437, 2.134, 2.080) are close to the rigid lattice limit values for $Cu^{2+}(H_2O)_6$ found in other EPR studies of doped Tutton salt systems (average: g_{max} = 2.438, g_{mid} = 2.123, g_{min} = 2.056)[1,2,4,7,9,10], and pure copper Tutton salts (average: g_{max} = 2.430, g_{mid} = 2.112, g_{min} = 2.062)[2,14]. The three Cu-OW distances in CdCrnS are assumed to adopt values close to the average of copper Tutton structures (average: 2.296, 2.032, 1.963 Å)[2]. The difference between these and the Cd-water bond lengths in Figure 6 illustrate the extent of local structural adaptation the host lattice undergoes to accommodate the copper.

The EPR powder spectra observed and simulated at 295 K and 110 K are pictured in Figure 7. The spectra show a small increase in g_{max} (from 2.448 to 2.462), a decrease in g_{mid} and a large reduction in linewidth as the temperature decreases. EasySpin[38] simulations match the spectra using **g**; 2.448, 2.125, 2.085, $\mathbf{A}^{Cu}$; -315, -75.0, 35.0 MHz, gaussian linewidth≈57 G, for room temperature and **g**; 2.462, 2.116, 2.077, $\mathbf{A}^{Cu}$; -340, -30.0, 35.0 MHz, gaussian linewidth≈22 G, for 110 K. These are

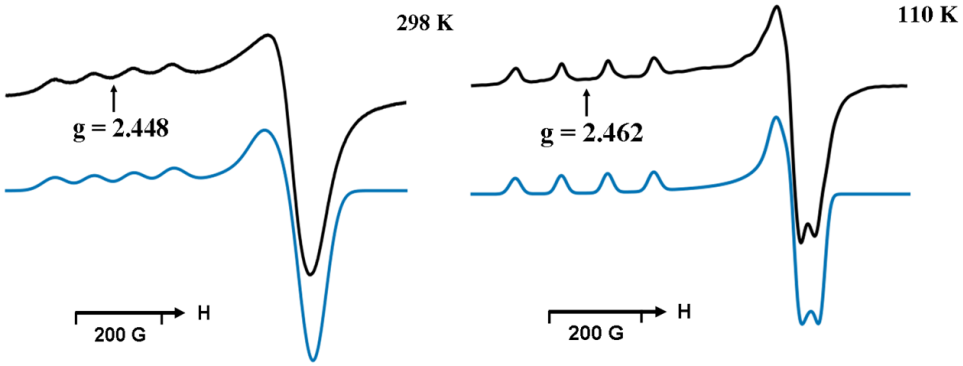

Figure 7

listed in Table 2. The room temperature powder values agree reasonably well with the tensors obtained from single crystal measurements, that is, within the uncertainty inherent when comparing spectra from the two different sample types[28]. The small temperature variation of **g** and $\mathbf{A}^{Cu}$ is expected since these are already close to the rigid lattice limits even at room temperature. This contrasts with the large temperature dependences observed for the tensors in copper hexahydrate containing crystals[1-3].

For further examination, a CdCrnS crystal was orientated in the **bc'** plane so that the g_{max} for one the copper complexes was nearly aligned with the external field (the angular deviation between the two was less than 20°). Figure 8 depicts the EPR spectra acquired from this orientation at 295 K and 77 K. A small increase of g_{max} from 2.436 to 2.447 contrasts the large decrease in linewidth from ~35 G to ~10 G as the temperature is decreased. Figure S1 displays the EPR spectra for this crystal orientation at intervals from 295 K down to

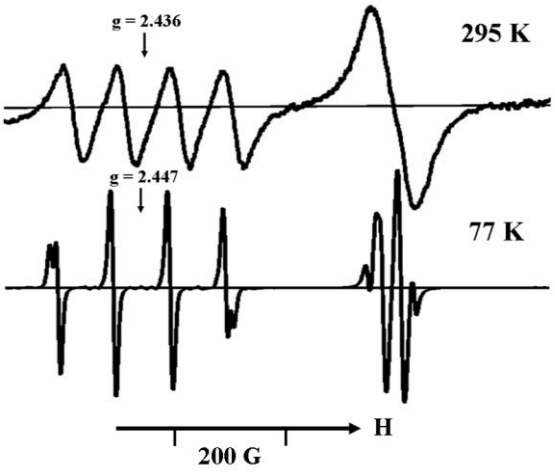

Figure 8

77 K. The low field quartet pattern g value and copper hyperfine coupling parameters were fit using EasySpin[38] adopting a gaussian linewidth for the individual lines. Using the low field m_I=1/2 peak, the linewidth dependence on temperature is plotted in Figure 9 and is analyzed below. Likewise, the g value of this low field pattern was determined at the different temperatures and its variation is traced by the triangles in Figure 10. These observations will be discussed later.

Discussion

The aims of this investigation are to determine the crystal structure of a metal organic hybrid analog of Tutton's salt and to gain further understanding on the relationship between dynamics and the electronic nature of copper-hexahydrate. The EPR measurements reveal both common and distinct features for $Cu^{2+}(H_2O)_6$ in CdCrnS compared to other similar systems. A significant linewidth dependence with temperature in CdCrnS is one feature shared by all copper doped Tutton salts.

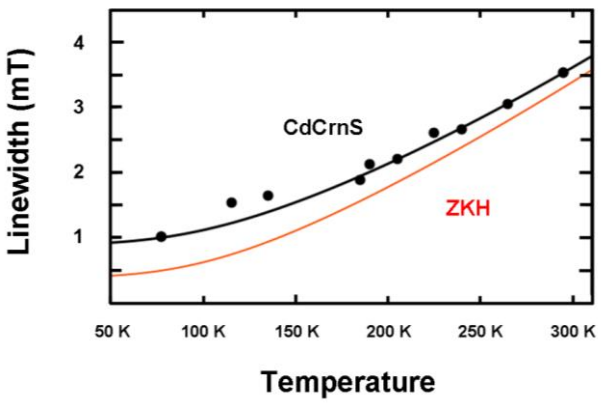

Figure 9

The analysis of the EPR linewidth (ΔB) variation of CdCrnS follows Hoffmann and Goslar (HG)[53] who considered that line broadenings mainly come from two independent temperature dependent mechanisms[53,54]. Above 15 K, the spin-lattice relaxation (T_1) is the primary broadening mechanism[20,53-55] but this becomes secondary at temperatures greater than ~150 K[53]. There the affect of the reorientation between Jahn-Teller configurations was proposed as the dominant relaxation and broadening mechanism[53]. The former process is governed by the two-phonon Raman process[20,53-55]. The later depends on the jump rate τ and energy difference (δ_{12lw}) between the two lowest configurations[53,54]. The lifetime in the individual states is believed to approach 10^{-9}s at room temperature. For CdCrnS, the measured temperature dependence of ΔB using the copper m_I=1/2 line of the g_{max} pattern (see Figure S1) was fit to formulas derived by HG using the natural linewidth (ΔB_o), τ and δ_{12lw} as adjustable parameters. The quantities describing the Raman process, specifically with b=0 and a Debye Temperature of 166 K, were taken from the previous analysis of copper-doped zinc potassium sulfate hexahydrate (ZKH)[53]. The curves depicted in Figure 9 were computed using formulas described in Table S13, with fit parameters ΔB_o = 0.9 mT, τ = 1.2e9s^{-1} and δ_{12lw} = 265 cm^{-1} for CdCrnS (black line), and with ΔB_o = 0.4 mT, τ = 0.6e9s^{-1} and δ_{12lw} = 167 cm^{-1} for ZKH (red). Both curves are quite similar,

except perhaps for a small difference in natural linewidth. A qualitative comparison of δ_{12lw} indicates a much larger energy gap between the JT configurations for CdCrnS than ZKH. However, the δ_{12lw}'s found by analyzing linewidth broadenings have been found to have a very poor correspondence to the δ_{12}'s determined from the SG or vibronic models of g tensor variations. Close agreement of δ_{12} derived from the two approaches have been found in only one system, Cu^{2+}-doped $Mg^{2+}(NH_4)_2(SO_4)_2{\cdot}6H_2O$ [4]. The large disparity found again here for CdCrnS (δ_{12lw}=265cm^{-1} versus δ_{12}=640cm^{-1} using the SG model, see below) suggests the presence of other broadening processes.

EPR of CdCrnS shows only small variations of the **g** and $\mathbf{A^{Cu}}$ tensors with temperature. Even so, they are significant enough to be analyzed at X-band frequency. As the temperature is decreased below room temperature, the g_{max} (g_z) value (and $A^{Cu}{}_{max}$, not shown) increases, g_{mid} (g_y) decreases and g_{min} (g_x) is relatively constant. This is the typical trend for copper hexahydrate complexes in doped Tutton salts[1-3], but for CdCrnS the magnitude of these variations is much reduced. The reason is that a large static distortion exists in CdCrnS but with enough instability to foster a small temperature dependent averaging of the **g** and $\mathbf{A^{Cu}}$ tensors. The variation of the powder **g** values is shown in Figure 10 at 298 K and 100 K. Also plotted are the "near" g_{max} values (triangles) obtained from the oriented crystal from 295 K to 77 K (see Figure S1). These data parallel the powder parameter measurements. The black curves display a good fit to the data using the two-state SG model with δ_{12} = 640 cm^{-1}. This is the largest δ_{12} reported for any copper hexahydrate complex and is rivaled only by the $Cu(HCOO)_6$ complex in doped cadmium formate dihydrate, where a similar SG analysis found $\delta_{12}\approx$520 cm^{-1} [56]. Included in the Figure for comparison are the g variation curves (red) derived from the study of ZKH[1] with δ_{12}=75 cm^{-1}.

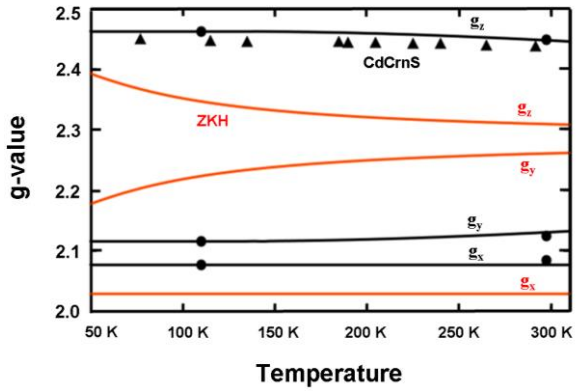

Figure 10

Table 3 provides the EPR magnetic parameters for copper doped Tutton salts and analogs crystals, as well as the energy separation between the two lowest JT configurations in these systems. A comparison of the results appears to show a relationship between the tensor x components, i.e., g_{min} and A^{Cu}_{x}, and the δ_{12} values determined from a SG analysis. These are displayed in Figure 11. In general, an increase in g_x, and a decrease in A^{Cu}_{x}, weakly correlates with a larger δ_{12}. Not all systems follow this trend and the three exceptions are the two ammonium sulfate salts (Mg and Zn) and Tutton analog $Zn^{2+}Cs_2(H_2O)_6(ZrF_6)_2$ (red points). As discussed above, these specific systems were reported to have clear deviations from predictions using both the simple SG and vibronic models[4,11,18,20,21]. The remaining ones suggest a common electronic origin. One possibility for this lies in parameters that define the copper d_{x2-y2} and d_{z2} orbital contributions to the unpaired wavefunction. Hitchman[57] and later with Waite[58] were able to assess these quantities in copper model compounds and copper Tutton salts by first considering an elongated octahedral complex, with orbital x, y and z lobes being directed along the g_x (g_{min}), g_y (g_{mid}) and g_z (g_{max}) directions. Then by expressing the copper hybrid d_{z2} and d_{x2-y2} ground state wavefunction as $\Psi = |cx^2 + ey^2 + fz^2>$, the orbital lobes along the x, y and z axes become inequivalent. With this scheme they[57,58] were able to deduce the unpaired spin

populations in the separate lobes by relating measured g-tensors to the wavefunction parameters for a series of copper model compounds. In a qualitative sense an increase in the amount spin in the x-lobe would lead to a decreased g_x-value and an increase in A^{Cu}_x since the hybrid function would contain more 'unique" character along x, or in other words, more "d_{x2-r2}" mixing into the ground state[57-60]. This representation can help explain the trends in Figure 11.

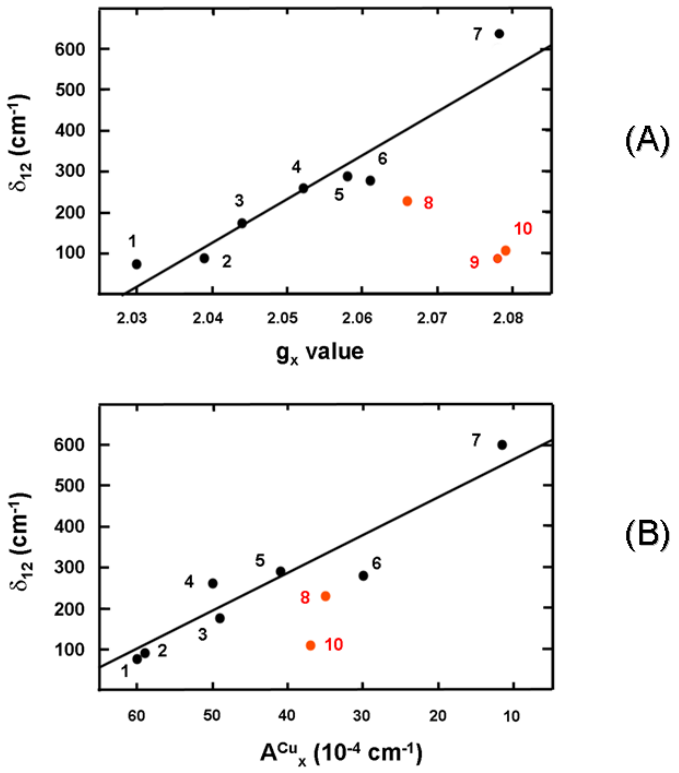

Figure 11

Using the rigid lattice g tensors for the doped Tutton salts and two Tutton analogs listed in Table 3, along with the 110 K powder parameters for CdCrnS, the iterative routine outlined by Hitchman[58] was used to determine the copper unpaired wavefunction parameters and spin populations in the x, y and z lobes for these systems. In two cases of specific interest, the unequal spin percentages in the x, y and z lobes were 53.3%, 46.5% and 0.2%, respectively for CdCrnS and 60.3%, 36.7% and 2.9%, respectively for ZKH. By plotting δ_{12} versus the x-lobe

spin percentages derived for the systems in the Table, the apparent correspondence between the two is shown in Figure 12. An empirical curve $\delta_{12} = 4(65\text{-sdx})^2$, where sdx is the spin % in the x-lobe passes through most of the points. The outliers (red points) again are from the three systems which have been considered anomalous when applying both the SG and vibronic models; i.e., the Mg and Zn ammonium Tutton salts and the Tutton analog $Zn^{2+}Cs_2(H_2O)_6(ZrF_6)_2$.[4,11,18] For the other systems Figure 12 tentatively suggests that as the spin probability in the x-lobe increases, the separation between the lowest two potential wells become smaller. Conceptually, an increase in x spin density means the unpaired orbital adopts more "$d_{x2\text{-}r2}$" character which should bring the y and z configurations closer together. The paucity of available data prevents making any definite conclusions. However, it is tempting to speculate that the trend in Figure 12 displays an approximate empirical relationship between the unpaired electron distribution and the δ_{12} of fluxional $Cu^{2+}(H_2O)_6$ systems.

This view is consistent in principle, by not extent, with a recent analysis of the affect of the internal electric field created by the lattice charges on the unpaired wavefunction in the copper-doped zinc potassium sulfate Tutton salt (ZKH)[61]. The authors argue that the internal field in the x-direction has enough affect to transform the unpaired electron distribution from the normally considered $d_{x2\text{-}y2}$ orbital into one predominantly $d_{z2\text{-}r2}$, where the z axis is now directed along shortest Zn/Cu-water bond, with ~25% in their $d_{x2\text{-}y2}$. However, comparing this and the hybrid wavefunction of Hitchman, the latter seems to be better at explaining the copper ligand hyperfine interactions. Lending support for an unequal spin distribution in the x and y lobes comes from examining how the copper bound ^{17}O-water couplings derived from the Hitchman spin densities compare to those previously measured in doped, enriched ZKH. For this system, the relative isotropic ^{17}O couplings (a_{iso}) computed using the x, y and z lobe spin densities listed

above give a_{iso}^{17O}: -16.2, -9.87, -0.74 G, which are in close agreement to their experimental counterparts found from EPR (-14.9, -11.6 G)[60] for the x and y equatorial ^{17}O-water couplings, respectively, and from pulsed-EPR (-0.41 G)[62] for the axial (z) ^{17}O-water coupling. Even so, for either representation the effect of crystalline fields on the complex is an important factor not to be overlooked in determining the unpaired electron distribution and how it relates to the dynamic features of copper hexahydrate.

Conclusion

The crystal structure of copper doped cadmium creatininium sulfate has been determined by X-ray diffraction at 298 K and at 100 K temperatures. The structure is an analog of Tutton's salt, where the unit cell consists of creatininium cations, sulfates, Cd/Cu hexahydrate cations at inversion centers and solvation waters. The Cd/Cu site adopts a slightly distorted octahedral coordination geometry. This coordination of the metal site by six waters is like that seen in metal hexahydrate complexes of Tutton's salts and other structural analogs of them with organic cations. The structure is held together by a network of hydrogen bonds and stacking interactions.

The X-ray diffraction and EPR results show correspondence between the Cd-O water directions and the measured **g** tensor (and $\mathbf{A}^{\mathbf{Cu}}$ tensor) principal directions, where the g_{min}, g_{mid} and g_{ma} directions align with the smallest, middle and longest metal-water bonds in the cadmium host, respectively. The assignment of bonding length rank order of the host structure to the g tensor principal directions is consistent throughout the Tutton salt studies. It is also interesting that this rank also holds for Cd ammonium sulfate hexahydrate[8,9] and CdCrnS, where only small differences between the three Cd-water distances (Figure 6) are seen.

Past EPR investigations of copper hexahydrate in doped Tutton crystals and similar analogs have reported temperature dependent averaging of the spectra, which is attributed to the

dynamic Jahn-Teller effect. In this process vibrations mix the copper electronic states which in the SG model represent fast reorientations of the magnetic tensor axes of the $Cu^{2+}(H_2O)_6$ complex and lead to EPR spectral averaging. This dynamic model, developed by Silver and Getz[1], has been successfully utilized in numerous studies of Tutton systems to obtain estimates for the energy spacing between the three JT configurations. A study of the current system was therefore undertaken to characterize the dynamic behavior of copper hexahydrate in a metal organic hybrid analog of Tutton's salt.

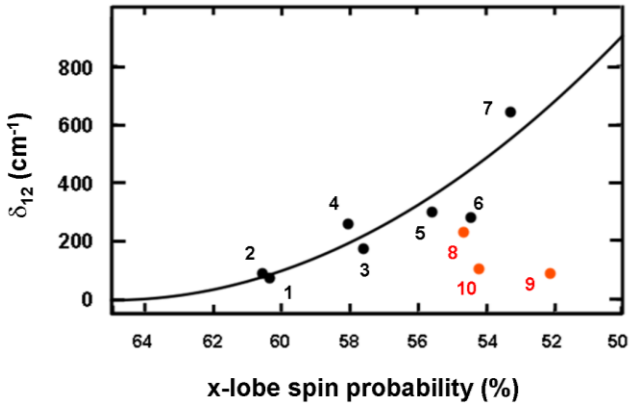

Figure 12

As shown by Tables 2 and 3, one unique feature found for this system is that the room temperature **g** and $\mathbf{A}^{Cu}$ tensor values are close to those found at low temperatures in the doped Tutton salts. This observation of the near rigid lattice tensor values at room temperature in CdCrnS demonstrates a large static interaction at the copper site. However, the small shifting of tensors with temperature also indicates the presence of a dynamic process. The two-state SG model analysis of the **g** variation with temperature gives an estimate for the energy gap between the lowest and next highest potential well of 640 cm^{-1}. The δ_{12} determined here is much greater than those found in doped Tutton salts and is more akin to those obtained from the pure copper Tutton salts. This could mean that CdCrnS host is better able to accommodate distortions

induced by the copper than in the Tutton salts. The structure of the pure copper creatininium sulfate may provide insight on this point. This study was also undertaken to shed light on structural and electronic factors that may affect dynamic processes in this system. Results from similar systems suggest that the spin population in the x-lobe may be a sensitive indicator of the energy separation between the JT configurations. However, the role of unbalanced equatorial spin density on dynamics in these systems needs further clarification.

This work reflects the first opportunity to evaluate copper dynamic behavior in a metal organic hybrid analog of Tutton's salt. The major difference observed between the behavior of CdCrnS and all other doped Tutton systems is the nearly static copper-hexahydrate site, which in terms of the SG model, gives a very large separation between JT configuration energies. The reason for this is currently unknown. This initial EPR study of a copper hexahydrate complex in a metal organic hybrid crystal will hopefully spur additional interest in similar systems.

Supporting Information

Tables S1−S6 (crystallographic data) for the 298 K structure and Tables S7−S12 (crystallographic data) for the 100 K structure and Figure S1 for temperature dependent EPR spectra of an oriented crystal from 295 K to 77 K and Table S13 which describes the method used in analyzing the EPR linewidth dependence on temperature (PDF)

CIF file for the 298 K (rt_a.cif) structure (CIF)

CIF file for the 100 K (100k_a.cif) structure (CIF)

This information is available free of charge via the Internet at http://pubs.acs.org

CCDC references 1981649; 1981650 contain the supplementary crystallographic data for this paper. The data can be obtained free of charge from The Cambridge Crystallographic Data Centre via www.ccdc.cam.ac.uk/structures.

Acknowledgements

This research used resources of the Advanced Light Source, which is a DOE Office of Science User Facility under contract no. DE-AC02-05CH11231. The Chimera program is developed by the Resource for Biocomputing, Visualization, and Informatics at the University of California,

San Francisco (supported by NIGMS P41-GM103311).

References

(1) Silver, B.L.; Getz, D. ESR of $Cu^{2+}(H_2O)_6$. II. A Quantitative Study of the Dynamic Jahn-Teller Effect in Copper-Doped Zinc Tutton's salt. *J. Chem. Phys.* **1974**, *61*, 638-650.

(2) Petrashen, V.E.; Yablokov, Yu.V.; Davidovich, R.L. The Lattice Structure Parameters and Configuration of Cu^{2+} Jahn-Teller Centres in Tutton Salt Crystals. *Phys. Status Solidi B* **1980**, *101*, 117-125.

(3) Riley, M.J.; Hitchman, M.A.; Mohammed, A.W. Interpretation of the Temperature Dependent g Values of the $Cu(H_2O)_6^{2+}$ ion in Several Host Lattices Using a Dynamic Vibrational Coupling Model. *J. Chem. Phys*. **1987**, *87*, 3766-3778.

(4) Hoffmann, S.K.; Goslar, J.; Hilczer, W.; Augustyniak, M.A.; Marciniak, M. Vibronic Behavior and Electron Spin Relaxation of Jahn-Teller Complex $Cu(H_2O)_6^{2+}$ in $(NH_4)_2Mg(SO_4)_2 \cdot 6H_2O$ Single Crystal. *J. Phys. Chem. A* **1998**, *102*, 1697-1707.

(5) Tregenna-Piggot, P.L.W; Riley, M.J. Constructing, Solving and Applying the Vibronic Hamiltonian. in *The Jahn-Teller Effect*; Koppel, H., Yarkony, D.R., Barentzen, H., Eds.: Springer: New York, **2009**; 371-413.

(6) O'Brien, M.C.M. The Dynamic Jahn-Teller Effect in Octahedrally Co-ordinated d9 Ions. *Proc. R. Soc. London Ser. A.* **1964**, *281*, 323-339.

(7) Atherton, N.M.; Horsewill, A.J. Proton ENDOR of $Cu(H_2O)_6^{2+}$ in $Mg(NH_4)_2(SO_2)_4 \cdot 6H_2O$. *Mol. Phys.* **1979**, *37*, 1349-1361.

(8) Satyanarayana, N. E.P.R. and Ground State Wavefunction Studies of Cu^{2+} Ion in $Cd(NH_4)_2(SO_4)_2 \cdot 6H_2O$ Single Crystals. *Mol. Phys.* **1985**, *55*, 111-119.

(9) Misra, S.K.; Wang, C. EPR of Cu^{2+}-Doped Cadmium Ammonium Sulfate: Pseudo-Jahn-Teller Effect. *Phys. Rev. B: Condens. Matter Mater. Phys.* **1990**, *41*, 1-7.

(10) Rao, P.S.; Viswanath, A.K.; Subramanian, S. EPR of Dynamic Jahn-Teller Distortion in Cu^{II} Doped Magnesium Tutton's Salt. *Spectrochim. Acta A* **1992**, *48*, 1745-1757.

(11) Augustyniak, M.A.; Usachev, A. E. The Host Lattice Influence on the Jahn-Teller Effect of the $Cu(H_2O)_6^{2+}$ Complex Studied by EPR in $K_2Zn(SO_4)_2 \cdot 6H_2O$ and $(NH_4)_2Zn(SO_4)_2 \cdot 6H_2O$ Tutton Salt Crystals. *J. Phys.: Condens. Matter* **1999**, *11*, 4391-4400.

(12) Hoffmann, S.K.; Kaszynski, R.; Augustyniak, M.A.; Hilczer, W. Restricted Validity of the Two-Ste Model Describing a Vibronic EPR g-Factors Averaging in $Cs_2Zn(SO_4)_2 \cdot 6H_2O$ Tutton Salt Crystals Doped with Cu^{2+} Ions. *Acta Phys. Pol. A* **1999**, *96*, 733-740.

(13) Hoffmann, S.K.; Gomolka-Marciniak, M. Vibronic Effects in EPR Spectra of $(NH_4)_2Cu(BeF_4)_2 \cdot 6H_2O$ Single Crystal. *Acta Phys. Pol. A* **1993**, *83*, 817-830.

(14) Marciniak, M.; Hoffmann, S.K.; Augustyniak, M.A.; Hilczer, W. Comparative EPR studies of Dynamics and Exchange Coupling in Ammonium and Potassium Copper(II) Tutton Salts. *Phys. Status Solidi B* **1995**, *191*, 201-215.

(15) Hitchman, M. A.; Maaskant, W.; van der Plas, J.; Simmons, C.J.; Stratemeier, H. Cooperative Jahn-Teller Interactions in Dynamic Copper(II) Complexes. Temperature Dependence of the Crystal Structure and EPR Spectrum of Deuterated Ammonium Copper(II) Sulfate Hexahydrate. *J. Am. Chem. Soc.* **1999**, *121*, 1488-1501.

(16) Augustyniak-Jablokow, M.A.; Yablokov, Yu.V, The Pair Exchange Interaction and Jahn-Teller Correlations of $Cu(D_2O)_6^{2+}$ Centres in Some Tutton Salt Crystals. *Solid State Commun.* **2000**, *115*, 439-443.

(17) Petrashen, V. E.; Yablokov, Yu. V.; Davidovich, R. L. Electron Paramagnetic Resonance Study of Cu^{2+} in $K_2Zn(ZrF_6)_2 \cdot 6H_2O$. *Phys. Status Solidi B* **1978**, *88*, 439-443.

(18) Hitchman, M. A.; Yablokov, Yu.V.; Petrashen, V.E.; Augustyniak-Jablokow, M.A.; Stratemeier, H.; Riley, M.J.; Lukaszewicz, K.; Tomaszewski, P.E.; Pietraszko, A. Dynamic Behavior of the Jahn-Teller Distorted $Cu(H_2O)_6^{2+}$ Ion in Cu^{2+} Doped $Cs_2[Zn(H_2O)_6](ZrF_6)_2$ and the Crystal Structure of the Host Lattice. *Inorg. Chem.* **2002**, *41*, 229-238.

(19) Hadler, K.S.; Kilmartin, J.R.; Hanson, G.R.; Hitchman, M.A.; Simmons, C.J.; Riley, M.J. Vibronic Effects in Cu(II)-Doped $Ba_2Zn(HCO_2)_6 \cdot 4H_2O$. *Inorg. Chem.* **2008**, *47*, 8188-8196.

(20) Hoffmann, S.K.; Goslar, J.; Hilczer, W.; Augustyniak-Jublokow, M.A. Electron Spin Relaxation of Vibronic $Cu(H_2O)_6$ Complexes in $K_2Zn(SO_4)_2 \cdot 6H_2O$ Single Crystals. *J. Phys.: Condens. Matter* **2001**, *13*, 707-718.

(21) Simmons, C.J.; Hitchman, M.A.; Stratemeier, H. Influence of Deuterium on the Crystal Structure of $(NH_4)_2Zn(H_2O)_6(SO_4)_2$. *Inorg. Chem.* **2000**, *39*, 6124-6126.

(22) Bacci, M.; Cannistraro, S. Temperature Dependence of the g Values in Blue Copper Protein EPR Spectra. *Chem. Phys. Lett.* **1987**, *133*, 109-112.

(23) Bacci, M.; Cannistraro, S. Role of Vibronic Coupling and of Conformation Substrate Distribution in Determining the Features of Copper-Protein EPR Spectra. *Appl. Magn. Reson.* **1990**, *1*, 369-378.

(24) Matoba, Y.; Kumagai, T.; Yamamoto, A.; Yoshitsu, H.; Sugiyama, M. Crystallographic Evidence that the Dinuclear Copper Center of Tyrosinase is Flexible during Catalysis. *J. Biol. Chem.* **2006**, *281*, 8981-8990.

(25) Sendovski, M.; Kanteev, M.; Ben-Yosef, V. S.; Adir, N.; Fishman, A. First Structures of an Active Bacterial Tyrosinase Reveal Copper Plasticity. *J. Mol. Biol.* **2011**, *405*, 227-237.

(26) Matoba, Y.; Bando, N.; Oda, K.; Noda, M.; Higashikawa, F.; Kumagai, T.; Sugiyama, M. A Molecular Mechanism for Copper Transportation to Tyrosinase that is Assisted by a Metallochaperone, Caddie Protein. *J. Biol. Chem.* **2011**, *286*, 30219-30231.

(27) Colaneri, M. J., Vitali, J.; Kirschbaum, K. Electron Paramagnetic Resonance Spectroscopic Study of Copper Hopping in Doped Bis(L-Histidinato)Cadmium Dihydrate. *J. Phys. Chem. A* **2013**, *117*, 3414-3427.

(28) Colaneri, M. J.; Vitali, J. Copper Dynamics in Doped Metal Bis(histidine) Complexes. *J. Phys. Chem. A* **2014**, *118*, 4688-4694.

(29) Colaneri, M. J., Teat, S. and Vitali, J. Models for Copper Dynamic Behavior in Doped Cadmium D,L-Histidine Crystals: Electron Paramagnetic Resonance and Crystallographic Analysis. *J. Phys. Chem. A* **2015**, *119*, 11119-11127.

(30) Bruker (2014). APEX2, SAINT and SADABS. Bruker AXS Inc., Madison, Wisconsin, USA.

(31) Blessing, R.H. An Empirical Correction for Absorption Anisotropy. *Acta Crystallogr.* **1995**, *A51*, 33-38.

(32) Sheldrick, G.M. A Short History of SHELX. *Acta Crystallogr.* **2008**, *A64*, 112-122.

(33) Dolomanov, O.V.; Bourhis, L.J.; Gildea, R.J.; Howard, J.A.K.; Puschmann, H. OLEX2: A Complete Structure Solution, Refinement and Analysis Program. *J. Appl. Crystallogr.* **2009**, *42*, 339-341

(34) Farrugia, L.J. WinGX and ORTEP for Windows: An Update. *J. Appl. Crystallogr.* **2012**, *45*, 849-854.

(35) Pettersen, E.F.; Goddard, T.D.; Huang, C.C.; Couch, G.S.; Greenblatt, D.M.; Meng, E.C.; Ferrin, T.E. UCSF Chimera--A Visualization System for Exploratory Research and Analysis. *J. Comput. Chem.* **2004**, *25*, 1605–1612.

(36) Wertz, J. E.; Bolton, J. R. In *Electron Spin Resonance: Elementary Theory and Practical Applications*; McGraw-Hill, Inc.: New York, **1972**.

(37) Tarvin, J.T. *An ENDOR Study of the Oxygen-17 Enriched Hexahydrated Copper(II) Complex in Lanthanum Magnesium Double Nitrate.* Ph.D. Dissertation, University of Kansas, Kansas City, Kansas, **1977**.

(38) Stoll, S.; Schweiger, A. EasySpin: A Comprehensive Software Package for Spectral Simulation and Analysis in EPR. *J. Magn. Reson.* **2006**, *178*, 42-55.

(39) Bosi, F.; Belardi, G.; Ballirano, P. Structural Features in Tutton's Salts $K_2[M^{2+}(H_2O)_6](SO_4)_2$, with M^{2+} = Mg, Fe, Co, Ni, Cu, and Zn. *Am. Mineral.* **2009**, *94*, 74–82.

(40) Bednarchuk, T.J.; Kinzhybalo, V.; Pietraszko, A. Synthesis, Structure and Characterization of Five New Organically Templated Metal Sulfates with 2-Aminopyridinium. *Acta Crystallogr*. **2016**, *C72*, 432–441.

(41) Rekik, W.; Naili, H.; Mhiri, T.; Battaille, T. Piperazinediium Hexaaquazinc(II) Bis(sulfate): A Structural Analogue of Tutton's Salts. *Acta Crystallogr.* **2005**, *E61*, m629–m631.

(42) Lukianova, T.J.; Kinzhybalo, V.; Pietraszko, A. Crystal Structure of New Organically Templated Copper Sulfate with 2-Amino- Pyridinium. *Acta Crystallogr.* **2015**, *E71*, m191–m192.

(43) Saıd, S., Mhadhbi, N.; Hajlaoui, F.; Yahyaoui, S.; Norquist, A. J. ; Mhiri. T.; Bataille, T.; Naıli, H. The Structural Transformation of Monoclinic [(R)-$C_5H_{14}N_2$] [$Cu(SO_4)_2(H_2O)_4$] $2H_2O$ into Orthorhombic [(R)-$C_5H_{14}N_2]_2$. *Phase Transitions* **2014**, *87*, 71–84.

(44) Honda, K.; Yamawaki, H.; Fujihisa, H.; Matsunaga, T.; Matsukawa, M. Hexaaquazinc(II) Dipicrate Trihydrate. *Acta Crystallogr.* **2007**, *C63*, m423-m426.

(45) Montgomery, H.; Lingafelter, E.C. The Crystal Structure of Tutton's Salts. IV. Cadmium Ammonium Sulfate Hexahydrate. *Acta Crystallogr.* **1966**, *20*, 728-730.

(46) Bahadur, S.A.; Rajalakshmi, M.; Athimoolam, S.; Kannan, R.S.; Ramakrishnan, V. Chain and Ring Motifs in Bis(creatininium) Sulfate. *Acta Crystallogr.* **2007**, *E63*, o4195.

(47) Messai, A.; Direm, A.; Benali-Cherif, N.; Luneau, D.; Jeanneau, E. Creatininium Perchlorate. *Acta Crystallogr.* **2009**, *E65*, o460.

(48) Bahadur, S.A.; Kannan, R.S.; Sridhar, B. Creatininium Hydrogen Oxalate Monohydrate. *Acta Crystallogr.* **2007**, *E63*, o2387– o2389.

(49) Bahadur, S.A.; Sivapragasam, S.; Kannan, R.S.; Sridhar, B. Creatininium Benzoate. *Acta Crystallogr.* **2007**, *E63*, o1714–o1716.

(50) Berrah, F.; Lamraoui, H.; Benali-Cherif, N. Hydrogen Bonding in Creatininium Nitrate. *Acta Crystallogr.* **2005**. E61, o210-o212

(51) Schottel, B.L.; Chifotides, H.T.; Dunbar, K.R. Anion-π Interactions. *Chem. Soc. Rev.* **2008**, *37*, 68-83.

(52) Lucas, X.; Bauzá, A.; Frontera, A.; Quiñonero, D. A Thorough Anion–π Interaction Study in Biomolecules: On the Importance of Cooperativity Effects. *Chem. Sci.* **2016**, *7*, 1038-1050.

(53) Hoffmann, S.K.; Goslar, J. Electron Spin Relaxation of Copper(II) Ions in Diamagnetic Crystals. *Appl. Magn. Reson.* **1998**, *14*, 293-303.

(54) Hoffmann, S.K.; Goslar, J. Effects of Vibronic Dynamics of $Cu(H_2O)_6$ Complexes and Electron Spin Relaxation in Temperature Dependence of EPR Linewidth in Diamagnetic Tutton Salt Single Crystals. *Acta Phys. Pol.* A **2006**, *110*, 807-816.

(55) Hoffmann, S.K.; Hilczer, W.; Goslar, J.; Augustyniak-Jublokow, M.A. Raman Spin-Lattice Relaxation, Debye Temperature and Disorder Effects Studied with Electron Spin Echo of Cu^{2+} in Tutton Salt Crystals. *J. Phys.: Condens. Matter* **2001**, *13*, 7443-7457.

(56) Kiezka, S.; Hoffmann, S.K.; Goslar, J.; Szczepanska, L. Electronic Structure, Jahn-Teller Dynamics and Electron Spin Relaxation of Two Types of Octahedral Cu(II) Complexes in Cadmium Formate Dihydrate $Cd(HCOO)_2 \cdot 2H_2O$. EPR and ESE studies. *Phys. Chem. Chem. Phys.* **2004**, *6*, 64-71.

(57) Hitchman, M.A. The Interpretation of Rhombic g Tensors in Copper Complexes. *J. Chem. Soc. A* **1970**, 4-9.

(58) Waite, T.D.; Hitchman, M.A. Molecular g Values of the $Cu(H_2O)_6^{2+}$ Ion. *Inorg. Chem.* **1976**, *15*, 2155-2158.

(59) Halcrow, M.A. Interpreting and Controlling the Structures of Six-Coordinate Copper(II) Centres - When is a Compression Really a Compression? *Dalton Trans.* **2003**, 4375-4384.

(60) Getz, D.; Silver, B.L. ESR of $Cu^{2+}(H_2O)_6$. I. The Oxygen-17 Superhyperfine Tensors in $^{63}Cu^{2+}$ Doped Zinc Tutton's Salt at 20° K. *J. Chem. Phys.* **1974**, *61*, 630-637

(61) Aramburu, J.A.; Bhowmik, A.; Garcia-Lastra, J.M.; García-Fernández, P.; Moreno, M. Insight into Compounds with $Cu(H_2O)_6^{2+}$ Units: New Ideas for Understanding Cu^{2+} in Tutton Salts. *J. Phys. Chem.* C **2019**, *123*, 3088-3101.

(62) Colaneri, M.J.; Vitali, J. Probing Axial Water Bound to Copper in Tutton Salt Using Single Crystal ^{17}O-ESEEM Spectroscopy. *J. Phys. Chem. A* **2018**, *122*, 6214-6224.

Table 1. Crystal data and refinement of the 100 K and 298 K structures.

	100 K	298 K
Empirical formula[1]	C8 H32 Cd0.96 Cu0.04 N6 O18 S2	
Formula weight[2]	674.96	
Wavelength, Å	0.7288	
Space group	$P2_1/n$	
Unit cell dimensions	a = 6.5282(2) Å	a = 6.5584(3) Å
	b = 27.7012(9) Å	b = 27.8708(12) Å
	c = 7.1557(2) Å	c = 7.1955(3) Å
	β= 110.584(1)°	β= 110.371(1)°
Volume	1211.42(6) $Å^3$	1232.99(9) $Å^3$
Z[3]	2	
Crystal size, mm^3	0.30 x 0.24 x 0.24	
Density (calculated), Mg/m^3	1.850	1.818
Absorption coefficient, mm^{-1}	1.231	1.209
Absorption correction	Semi-empirical from equivalents	
Maximum and minimum transmission	0.757 and 0.699	0.760 and 0.660
θ range for data collection	3.02 to 37.42°.	3.00 to 37.42°
Reflections collected	36926	47044
Independent reflections	5828 [R(int) = 0.0354]	5956 [R(int) = 0.0367]
Completeness to theta = 25.930°	99.3 %	99.9 %
Refinement method	Full-matrix least-squares on F^2	
Data / restraints / parameters	5828 / 0 / 218	5956 / 0 / 218
Goodness-of-fit on F^2	1.154	1.059
Final R indices[4] [I>2sigma(I)]	R1 = 0.0237, wR2 = 0.0576	R1 = 0.0218, wR2 = 0.0563
R indices[4] (all data)	R1 = 0.0243, wR2 = 0.0582	R1 = 0.0267, wR2 = 0.0582
Largest diff. peak and hole, $e.Å^{-3}$	0.681 and -0.705	0.543 and -0.559

[1] The empirical formula given corresponds to two asymmetric units related to each other by a crystallographic inversion center. Cd0.96/Cu0.04 is a mixed site at the inversion center. The asymmetric unit has one creatinine, one sulfate, three waters coordinated to the mixed Cd/Cu site at the inversion center and one additional water.
[2] The formula weight corresponds to the empirical formula.
[3] Z refers to the sum of two asymmetric units related by the crystallographic inversion center.
[4] $R_1 = \Sigma \, ||F_o| - |F_c|| / \Sigma |F_o|$; $wR_2 = [\Sigma[w (F_o^2 - F_c^2)^2] / \Sigma[w (F_o^2)^2]]^{1/2}$.

Table 2. The **g** and copper hyperfine coupling ($\mathbf{A}^{Cu}$) tensors obtained Cu(II)-doped cadmium creatinine sulfate crystals at room temperature (295K). The tensor principal directions (direction cosines) refer to the crystallographic **abc'** axes and are compared with the Cd-water directions in the structure. δ° are angular deviations between the **g** tensor and the Cu-water directions. Also listed are the powder **g** and $\mathbf{A}^{Cu}$ principal values determined at 295 K and 110 K.

		Principal Values	**Direction Cosines**			
			a	**b**	**c'**	
	z	2.437	0.2494	0.6982	0.6710	
g	**y**	2.134	0.5507	0.4677	-0.6913	
	x	2.080	0.7965	-0.5420	0.2679	
	z	-327.	0.1911	0.7068	0.6811	
$\mathbf{A}^{Cu}$ (MHz)	y	-84.8	0.4862	0.5346	-0.6912	
	x	7.33	0.8527	-0.4632	0.2415	
						δ°
	Cd-O(3)		0.2364	0.6754	0.6985	1.6
Cd-water	Cd-O(2)		0.4249	0.6135	-0.6657	7.9
	Cd-O(1)		0.8771	-0.4293	0.2155	6.0

Powder		**g**	$\mathbf{A}^{Cu}$ (MHz)
	z	2.448	-315.
295 K	**y**	2.125	-75.
	x	2.085	35.
	z	2.462	-340.
110 K	**y**	2.116	-30.
	x	2.077	35.

Table 3. Low temperature EPR magnetic parameters of copper hexahydrate in doped Tutton salt and analog crystal systems. The energy separation between the lowest and next highest JT configuration of the copper complex were derived in these studies from a SG model analysis.

Crystal System and study[a]	g values g_x	g_y	g_z	A^{Cu} (10^{-4} cm^{-1}) A^{Cu}_x	A^{Cu}_y	A^{Cu}_z	Temp	Energy Separation δ_{12} (cm^{-1})
ZKH	2.03	2.15	2.42	60	~20	96	4.2 K	75[b]
MgKS	2.039	2.205	2.387	59	31	71	77 K	90
ZnRbS	2.046	2.132	2.434	49	22	108	4.2 K	175
$CdNH_4S$	2.0513	2.1594	2.4290	52	26	112	4.2 K	260[c]
ZnCsS	2.058	2.121	2.444	38	~27	112	4.2 K	290[d]
ZnKSZrF	2.060	2.106	2.469	~30	~11	106	4.2 K	280[d]
CdCrnS	2.077	2.116	2.462	12	10	113	110 K	640
$ZnNH_4S$	2.067	2.122	2.430	~35	35	121	4.2 K	230[d]
ZnCsSZrF	2.077	2.100	2.506	-	-	-	4.2 K	90
$MgNH_4S$	2.07	2.12	2.42[e]	37	14	120[f]	4.2 K	108[f]

[a] system abbreviation: (ZKH)-$ZnK_2(SO_4)_2{\cdot}6H_2O$[1,3,11], (MgKS)-$MgK_2(SO_4)_2{\cdot}6H_2O$[10], (ZnRbS)-$ZnRb_2(SO_4)_2{\cdot}6H_2O$[2], (CdNH4S)-$Cd(NH_4)_2(SO_4)_2{\cdot}6H_2O$[8,9], (ZnCsS)-$ZnCs_2(SO_4)_2{\cdot}6H_2O$[2,12], (ZnKSZrF)-$ZnK_2(SO_4)_2{\cdot}6H_2O(ZrF_6)_2$[2,17], (CdCrnS)-current work, ($ZnNH_4S$)-$Zn(NH_4)_2(SO_4)_2{\cdot}6H_2O$[2,11], (ZnCsSZrF)-$ZnCs_2(SO_4)_2{\cdot}6H_2O(ZrF_6)_2$[18], ($MgNH_4S$)-$Mg(NH_4)_2(SO_4)_2{\cdot}6H_2O$[4,7]

[b] taken from Reference 1

[c] taken from Reference 9

[d] taken from Reference 2

[e] values taken from Reference 7

[f] values taken from Reference 4

Figure Captions

Figure 1. A view of the asymmetric unit at 298 K (A) and 100 K (B) with nomenclature for the non-hydrogen atoms. The asymmetric unit is augmented by three waters centrosymmetrically related to O1W, O2W and O3W and coordinated to the mixed Cd/Cu site at the inversion center. One may note the lower thermal motion of the 100 K structure. Figure was drawn with ORTEP-3.

Figure 2. The packing viewing along the **a** axis. Purple octahedra represent the metal cation, yellow tetrahedra the sulfates. The coloring scheme of the individual atoms is indicated. The structure consists of distinct organic (creatininium) double layers, sulfate layers and metal cation layers which are indicated. Figure was drawn with OLEX2.

Figure 3. Vertical interactions involving the creatininium cation. The planar cation (beige color) is sandwiched between the oxygens of the sulfate (yellow) at -1+x, y, z and O1 of an adjacent creatininium cation at ½ + x, 3/2 – y, ½ + z. The planes of the two symmetry related creatininium cations are at an angle of 81.97° (80.95° at 100 K) to each other. Shortest distances between the two rings involve O1 are O1---C1 3.006 Å (2.956 Å at 100 K), O1---C3 3.312 Å (3.274 Å at 100 K) and O1…N2 3.343 Å (3.306 Å at 100 K). Shortest distances of sulfate oxygens are O5 ---C1 3.305 A (3.262 Å at 100 K) O5---C3 3.385 Å (3.360 Å at 100 K) and O3---C2 3.285 Å (3.244 Å at 100 K). Figure was drawn using the Chimera software.

Figure 4. Single crystal X-band EPR spectra of Cu(II)-doped cadmium creatininium sulfate hexahydrate (CdCrnS) acquired at room temperature at the three reference orientations **a**//**H**, **b**//**H** and **c'**//**H**. The widths of individual copper m_I lines were roughly 35 G.

Figure 5. Plots showing the dependence of the copper EPR resonances on the crystal orientation as it is rotated in the external field. The points are the measured field values. The solid curves represent simulated values using Equation 1 and the best-fit **g** and $\mathbf{A}^{\mathbf{Cu}}$ hyperfine tensors listed in Table 2.

Figure 6. A view of the Cd/Cu hexahydrate complex in the structure of CdCrnS. Evidence that the copper replaces the cadmium in the hexahydrate complex comes from mixed occupancy treatment of the diffraction data. This is confirmed by single crystal EPR measurements which show good agreement between the metal-water directions and the g-tensor principle axes. The g_{min}, g_{mid} and g_{max} values are associated with the smallest, middle and longest Cd-water bonds, respectively. The deviations between these two sets of directions are labeled. The complex was drawn with Chimera.

Figure 7. X-band EPR powder spectra of CdCrnS measured at 298 K and 110 K. The blue curves are EasySpin simulations of the spectra using the powder parameters contained in Table 2. The g values marked in the Figure indicate the slight increase in g_{max} of the pattern as the temperature decreases.

Figure 8. The EPR spectra of a CdCrnS crystal at measured at 295 K and 77 K. The crystal was mounted along the **a** axis and oriented so the external field was nearly aligned (within ~20°) with

the g_{max} direction of one of the two copper complexes in the unit cell. EasySpin aided the determination of the g-value, copper hyperfine and linewidth of the patterns. These spectra are also repeated in Figure S1 along with those at a series of intermediate temperatures.

Figure 9. A plot of the linewidth of the m_I=+1/2 copper hyperfine line of the "near g_{max}" EPR pattern of CdCrnS displayed in Figure S1 as a function of temperature. The data points refer to the measured values. The black curve that fits the data was determined using the method described by HG[54] and in Table S13 with parameters ΔB_o = 0.9 mT, τ = 1.2e9s^{-1} and δ_{12lw} = 265 cm^{-1}. The red curve represents the theoretical fit reproduced from the EPR linewidth study of ZKH crystals[54] with parameters ΔB_o = 0.4 mT, τ = 0.6e9s^{-1} and δ_{12lw} = 167 cm^{-1}.

Figure 10. The variations of g tensor components as a function of temperature for CdCrnS and for ZKH. The dots are the powder measurements for CdCrnS in Table 2. The triangles are the measured g-values for the "near g_{max}" EPR pattern of the oriented CdCrnS crystal in Figure S1. The curves are variations predicted by the 2-state SG model formulas[1,2,11]: $g_z(T)= N_1g_{z1}+N_2g_{y1}$, $g_y(T)= N_1g_{y1}+N_2g_{z1}$ and $g_x(T)=g_{x1}$, where g_{z1}, g_{y1} and g_{x1} are the rigid lattice limit values for g_{max}, g_{mid} and g_{min}, respectively, and $N_1/N_2= \exp(\delta_{12}/kT)$, where $N_1+N_2=N=1$. The black curves fit the observations of CdCrnS with δ_{12}=640cm^{-1}. The red curves reproduce the temperature variation of the g values for ZKH found in SG[1] with δ_{12}=75cm^{-1}.

Figure 11. Plots showing the relationships between the difference in the first two levels of the potential energy surface (δ_{12}) and the rigid limit values for (A), the g_x (g_{min}) and (B), the A^{Cu}_x tensor components for $Cu^{2+}(H_2O)_6$ in copper doped Tutton salts and structural analogues. Systems are listed in Table 3 with 1-ZKH, 2-MgKS, 3-ZnRbS, 4-$CdNH_4S$, 5-ZnCsS, 6-ZnKSZrF, 7-CdCrnS, 8-$ZnNH_4S$, 9-ZnCsSZrF, 10-$MgNH_4S$

Figure 12. Graph showing a tentative correspondence between the differences in the first two levels of the potential energy surface (δ_{12}) and the d-orbital x-lobe spin probability determined using g-tensors as outlined by Hitchman[57] and with Waite[58] for Tutton salts and analogues. These systems are assigned as in Figure 11. The curve drawn is the hypothetical empirical function $\delta_{12}(cm^{-1}) = 4(65-x)^2$, with x = unpaired spin percentage, that traces the trend.

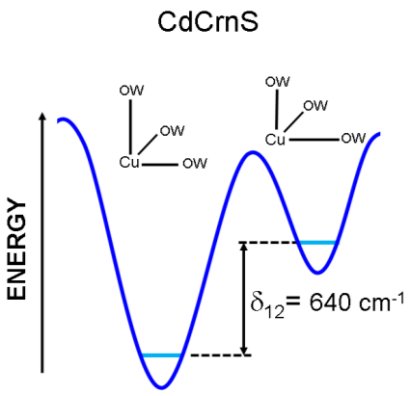

TOC Graphic